**Supplementary Information for**

# Synnovation and confluence explain disparities in species richness across the Andes and Hengduan-Himalaya Mountains

Chih-Chieh Yu, Zhi-Qiang Du, Shu-Feng Li, Renske E. Onstein, Richard H. Ree, Yao-Wu, Xing

**This PDF file includes:**



**Note:** Supplementary datasets, analysis outputs, and associated files supporting this study are available in the Figshare repository associated with this manuscript (DOI: 10.6084/m9.figshare.28288313).

Supplementary Note 1. **Biome and Habitat Delineation.**

The geographic boundary of the Hengduan–Himalayan Mountains (HHM) followed definition in Liu et al (1). Alpine and subalpine environments within the HHM were collectively treated as high-elevation habitats throughout the study. Because the elevation of the treeline ecotone varies substantially among mountain systems, ranging from approximately 1,800–2,300 m in the European Alps (2, 3), 3,300–4,300 m in the Pan–Tibetan highland (1, 4, 5), and 2,800–4,700 m in the Andes (6, 7), habitat classification was based on species' elevational distributions relative to the local climatic treeline rather than on absolute elevation.

Each *Berberis* species was assigned to a primary habitat category through a semi-quantitative assessment of elevational data and habitat information derived from herbarium records and iNaturalist observations. To ensure biological accuracy, we analyzed the frequency distribution of occurrence records relative to local treeline altitudes. Species consistently recorded entirely above the treeline ecotone were classified as alpine. For species with broader ranges, we applied a qualitative cross-validation using taxonomic monographs and regional floras to determine their primary ecological affinity. For instance, species whose distributions reached the treeline but were predominantly associated with forest-tundra transition zones (e.g., forest edges or subalpine shrublands) were classified as subalpine. Those primarily occurring in continuous montane forests, even if their upper limits approached the treeline, were categorized as non–alpine/subalpine. By prioritizing core elevational ranges over occasional outlier records, this integrated approach allowed for a robust classification that reflects the realized niche of each taxon within its respective mountain system. For state-dependent diversification analyses in Scenario 1 under the MuSSE framework, habitat was classified into montane versus non-montane categories based on core elevational distributions. Species primarily restricted to low elevations (0–200 m above sea level) or with upper elevational limits below 500 m were classified as non-montane, whereas all remaining species were treated as montane. To increase the robustness of this classification, we further validated montane assignments by intersecting occurrence records with the Global Mountain Biodiversity Assessment (GMBA) mountain inventory layer, which delineates mountain regions based on consistent topographic and environmental criteria (8). Species with occurrences falling within GMBA-defined mountainous terrain were retained as montane.

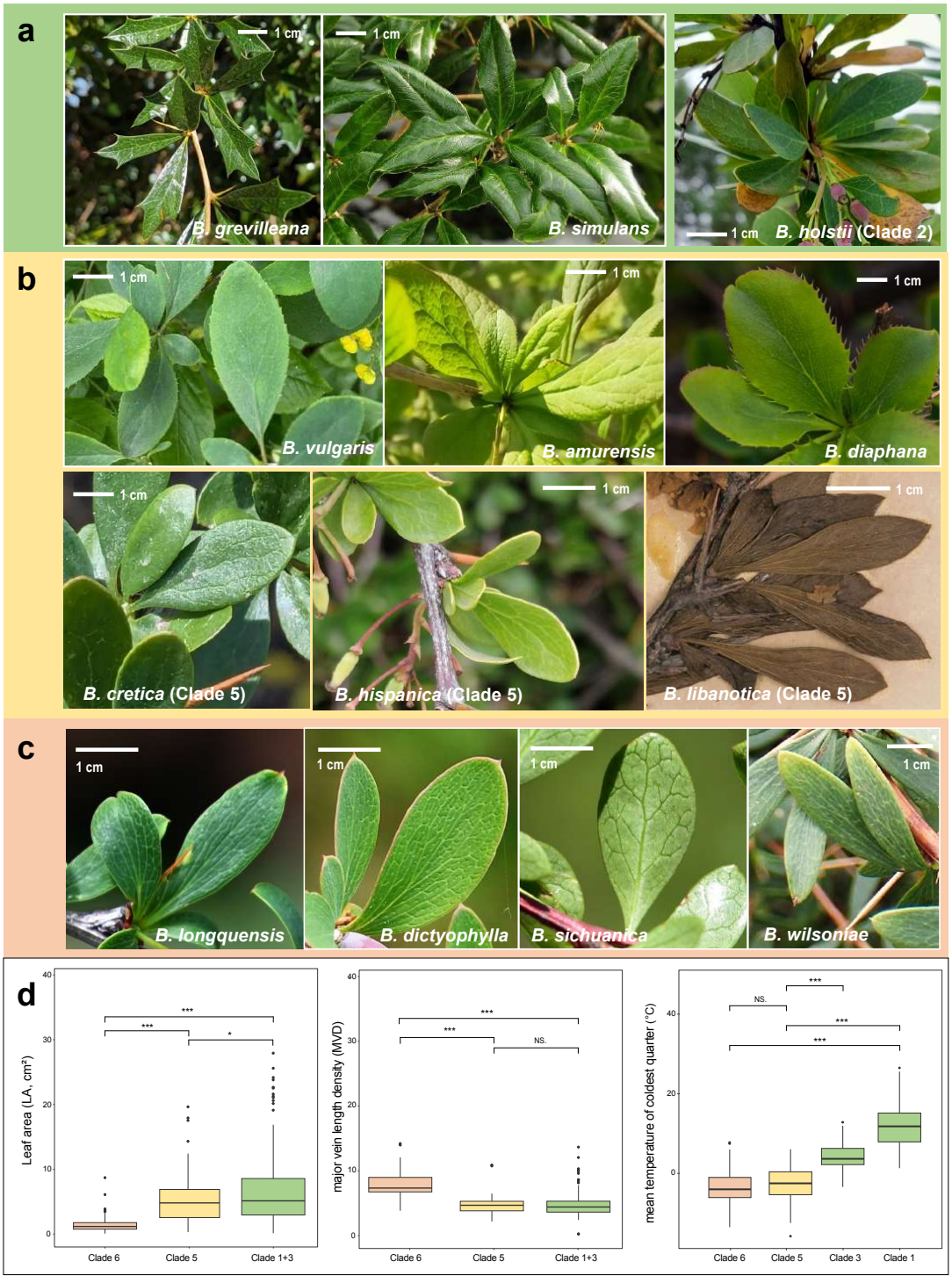


Supplementary Fig. 1. **Leaf morphology of *Berberis*: representative photographs and morphometric variation among major clades, with relationships to mean temperature of the coldest quarter. a.** Leaf morphology of selected evergreen species (Clades 1–3, corresponding to the clade numbering in Fig. 1). **b.** Representative leaf morphology of temperate deciduous species. Species in Clade 5a represent small, densely veined (SDV) leaf types occurring outside the Hengduan–Himalaya Mountains. **c.** Representative leaf morphology of deciduous species with small, densely veined (SDV) leaves from the Hengduan–Himalaya Mountains. **d.** Differences in leaf area, vein density, and mean temperature of the coldest quarter between evergreen and deciduous *Berberis*. Boxplots show the median (center line), interquartile range (box), and 1.5× interquartile range (whiskers), with points indicating outliers. Statistical differences among clades were evaluated using pairwise Welch t-tests in R. Asterisks indicate levels

of statistical significance (*$p$ < 0.05, **$p$ < 0.01, ***$p$ < 0.001), and NS denotes non-significant differences. Full statistical results, including test statistics, degrees of freedom, $p$ values, effect sizes, and 95% confidence intervals, are provided in Supplementary Table 14-16. Source data are provided as a Source Data file. Photo credits: The photograph of *B. holstii* in Panel **a** is reproduced from an iNaturalist observation by Mathew Rees (iNat Link; CC BY 4.0, https://creativecommons.org/licenses/by/4.0/). The photograph of *B. cretica* in panel b is reproduced from an iNaturalist observation by Marios Thoma (CC BY 4.0; iNat Link; CC BY 4.0, https://creativecommons.org/licenses/by/4.0/). The photograph of *B. hispanica* in Panel **b** is reproduced from an iNaturalist observation by Rafael Medina (CC BY 4.0; iNat Link; CC BY 4.0, https://creativecommons.org/licenses/by/4.0/). The specimen image of *B. libanotica* in Panel **b** is reproduced from the Herbarium Catalogue of the Royal Botanic Gardens, Kew (specimen K002120399; CC BY 4.0, https://creativecommons.org/licenses/by/4.0/).

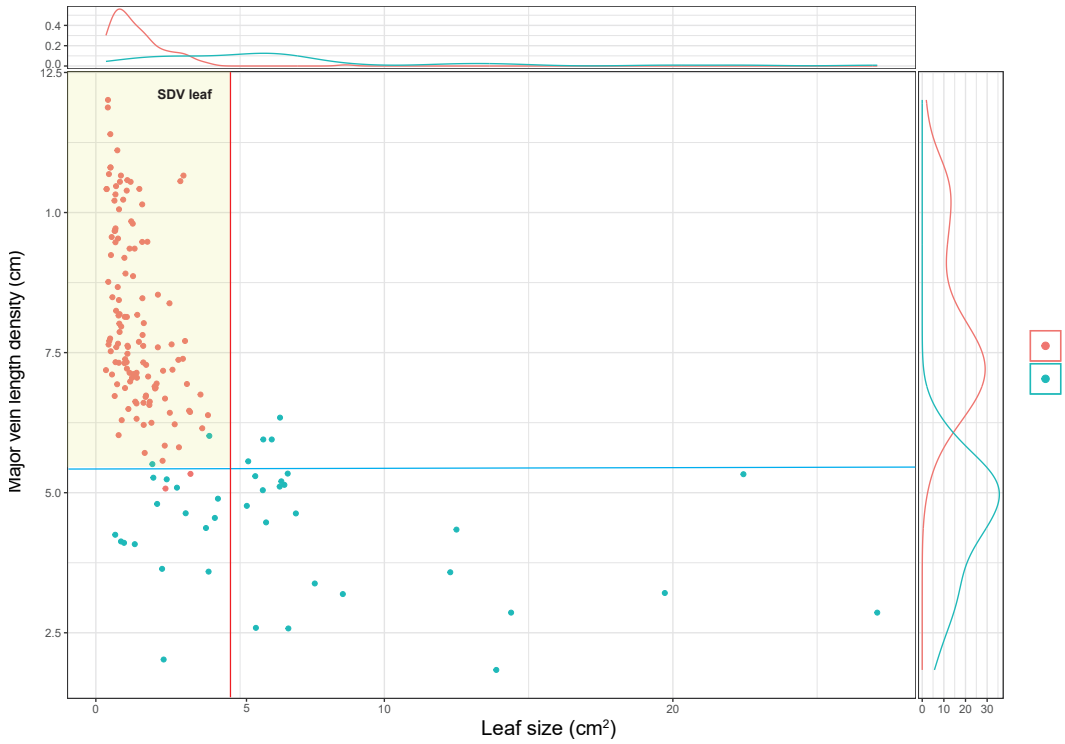


Supplementary Fig. 2. **Relationship between leaf area (LA) and density of major leaf vein (MVD) with the cut-off values.** The blue line represents the cut-off values for MVD, with blue dots marking the species of the Eurasian temperate Clade 5. Similarly, the red line indicates the cut-off values for LA, and red dots denote the species of the Hengduan-Himalaya deciduous Clade 6. *Berberis* taxa characterized by small, densely veined leaf (SDV leaf) are highlighted with a yellow box. Source data are provided as a Source Data file.

Supplementary Note 2. **Phylogenetic reconstruction and detecting incomplete lineage sorting and introgression.**

Prior to this study, phylogenetic relationships within *Berberis* were primarily inferred from Sanger-sequenced chloroplast fragments and nuclear ribosomal ITS data, with the exception of a recent plastome-based analysis focusing on a subset of species in Clade 3 (9). These studies were generally limited by incomplete taxon sampling (e.g., 10). In particular, the East African species were not included (with the exception of 11), and sampling of the Hengduan–Himalaya radiation remained sparse. Using genome-scale nuclear data, our phylogenomic analysis recovered five highly supported clades, with *Moranothamnus* consistently identified as the sister group to *Berberis*. To further assess the evolutionary relationships among these major clades, we selected 11 representative species to construct a backbone phylogeny. Specifically, two species were sampled from Clade 1 (*B. peruviana*, *B. darwinii*), and one species each from Clade 2 (*B. holstii*), Clade 3 (*B. lijiangensis*), Clade 6a (*B. angulosa*), and Clade 6b (*B. leboensis*). For Clade 5, three representative species were included (*B. amurensis*, *B. dictyoneura*, and *B. vulgaris*).

For these 11 taxa, complete plastome sequences were assembled. Raw reads were assembled into full chloroplast genomes using GetOrganelle v2.7.2 (12), with *B. amurensis* (MH926107.1) used as the reference. The plastid phylogeny was inferred under a maximum likelihood framework in IQ-TREE 3 using the MFP model. In parallel, the nuclear species-tree topology was inferred using ASTRAL-IV following the same procedure as for the full dataset. The resulting plastid phylogeny showed topological concordance with the backbone of the nuclear species tree. All major nodes in the plastid tree were strongly supported (ultrafast bootstrap = 100), while the corresponding nodes in the nuclear tree received maximal local posterior probability support (LPP = 1.0). The only exception was Clade 4, which showed lower support in the nuclear tree (LPP = 0.55).

To quantify the extent of incomplete lineage sorting (ILS) and introgression/ hybridization (IH), we re-ran ASTRAL backbone species tree, enabling quartet support counts (q1, q2, q3) with the *-u* 2 option. The resulting species tree and gene tree topologies were then analyzed using Phytop v1.1 (13) to compute node-specific ILS-index (ILS-i, 0–100%) and IH-index (IH-i, 0–50%), $\chi^2$ test *p*-values, and the proportions of discordant topologies attributable to ILS (ILS-e values) and IH (IH-e values). The ILS-i and IH-i indices quantify the strength of incomplete lineage sorting and introgression, respectively, at each internal node. A $\chi^2$ test was used to evaluate whether the imbalance between q2 and q3 could be explained by ILS alone or indicated additional IH. Visualization of these metrics was performed using Phytop's default settings, producing a species tree annotated with topology frequencies, ILS/IH indices, and node-specific phylogenetic conflict. To further examine the role of reticulation in observed discordance, we reconstructed explicit phylogenetic networks using SNaQ (14). SNaQ infers reticulation under a multispecies coalescent model by quartet concordance factors (qCFs). With the number of hybridization edges (hmax) increasing from 0 to 3, we performed 10 independent runs for each value of hmax. The nuclear backbone species tree served as the starting tree at hmax = 0. Then, for each subsequent hmax, the search began from the best-scoring network inferred at the previous hmax (i.e., hmax = 1). The optimal hybridization edge number was determined based on the degree of change in log-pseudolikelihoods between hmax values. The results and associated analysis files for the PhyTop and SNaQ analyses are available in the folder "1. Phylogenomic inference" at https://doi.org/10.6084/m9.figshare.28288313).

The ILS indices (ILS-i and IH-I) for nodes 1–4 was 75.6%/0%, 74.9%/0%, 93.9%/0%, and 97.6%/0%, respectively, indicating a high degree of incomplete lineage sorting across major nodes. The proportion of gene trees supporting the main topology exceeded 50% for nodes 1 and 2, but was reduced to approximately 35% for nodes 3 and 4. The best-fit hmax value inferred by SNaQ was 0, suggesting no significant introgression among the major clades, a result consistent with the findings from the Phytop analysis. It is noteworthy that in the nuclear backbone species tree, relationships among the major clades were recovered with strong support under the multispecies coalescent model (local posterior probability, LPP = 1.0 for all nodes except node 4), despite extensive incomplete lineage sorting (ILS). Such high support may reflect quartet-frequency asymmetries rather than genome-wide concordance (15). In the present SNP dataset, even with substantial proportions of conflicting quartets (ca. 50-65%), the

two alternative topologies were nearly equally represented, allowing ASTRAL to assign high LPP values.

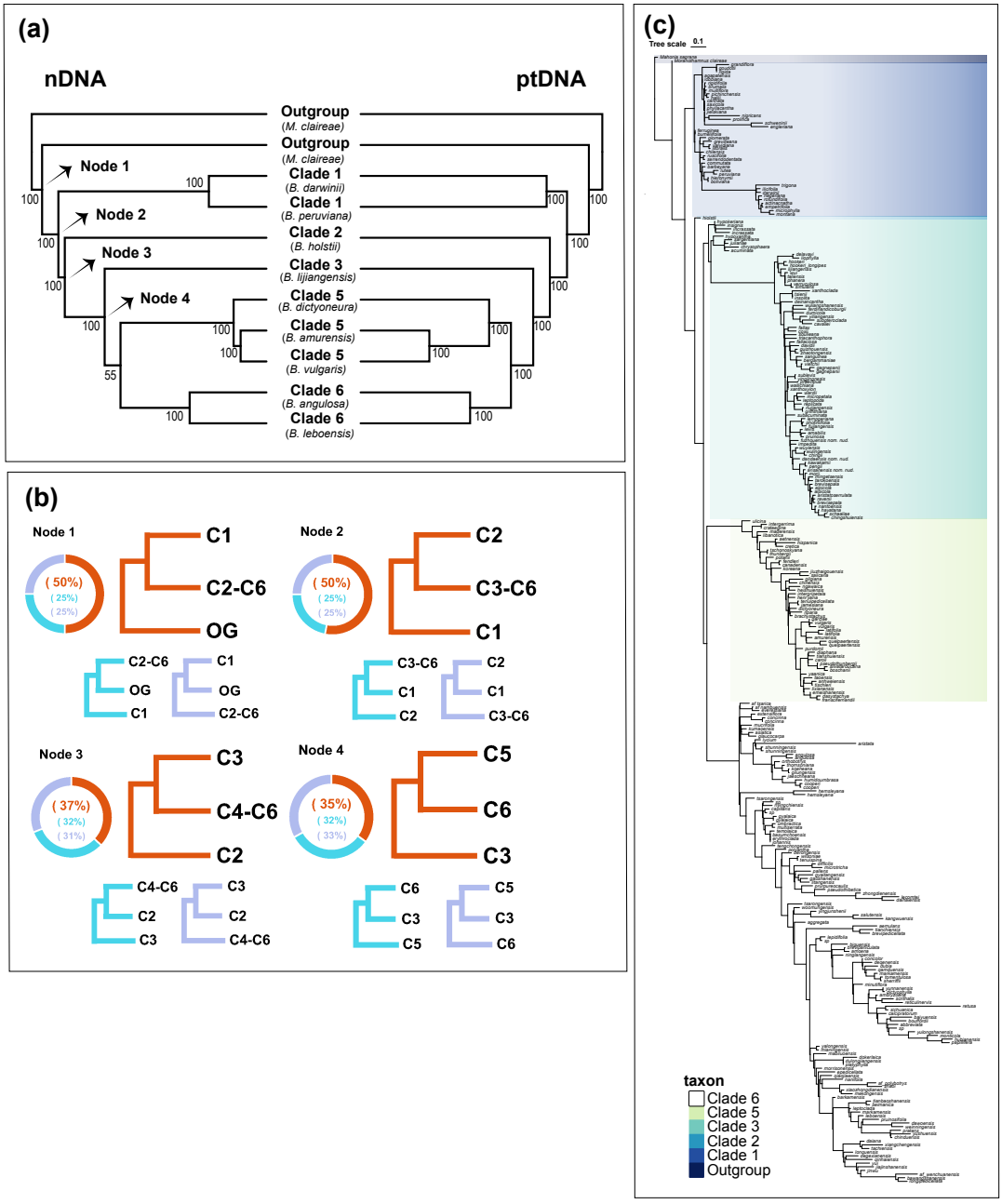


Supplementary Fig. 3. **ASTRAL-IV species tree with topology comparison between the nuclear (nDNA) and plastid (ptDNA) phylogenies, and results of the Phytop analysis based on the ASTRAL backbone species tree. a.** Comparison of nuclear and plastid phylogenies for representative taxa of *Berberis*. Values at major nodes indicate local posterior probabilities (LPP) and ultrafast bootstrap support, respectively. **b.** For each of the four key nodes (1–4) in the ASTRAL backbone species tree, the circular diagrams depict the proportions of gene trees supporting each of the three possible topologies. The dominant topology for each node (in orange) corresponds to the ASTRAL species tree, whereas the two alternative topologies (in blue and cyan) represent conflicting quartet relationships. The relative proportions indicate the frequency of gene tree support for each topology. "C" denotes the major *Berberis* clades (C1–C6). **c.** Species tree of *Berberis* inferred using ASTRAL-IV. The tree file with local posterior probability (LPP) values are available in the folder "1. Phylogenomic inference" at https://doi.org/10.6084/m9.figshare.28288313).

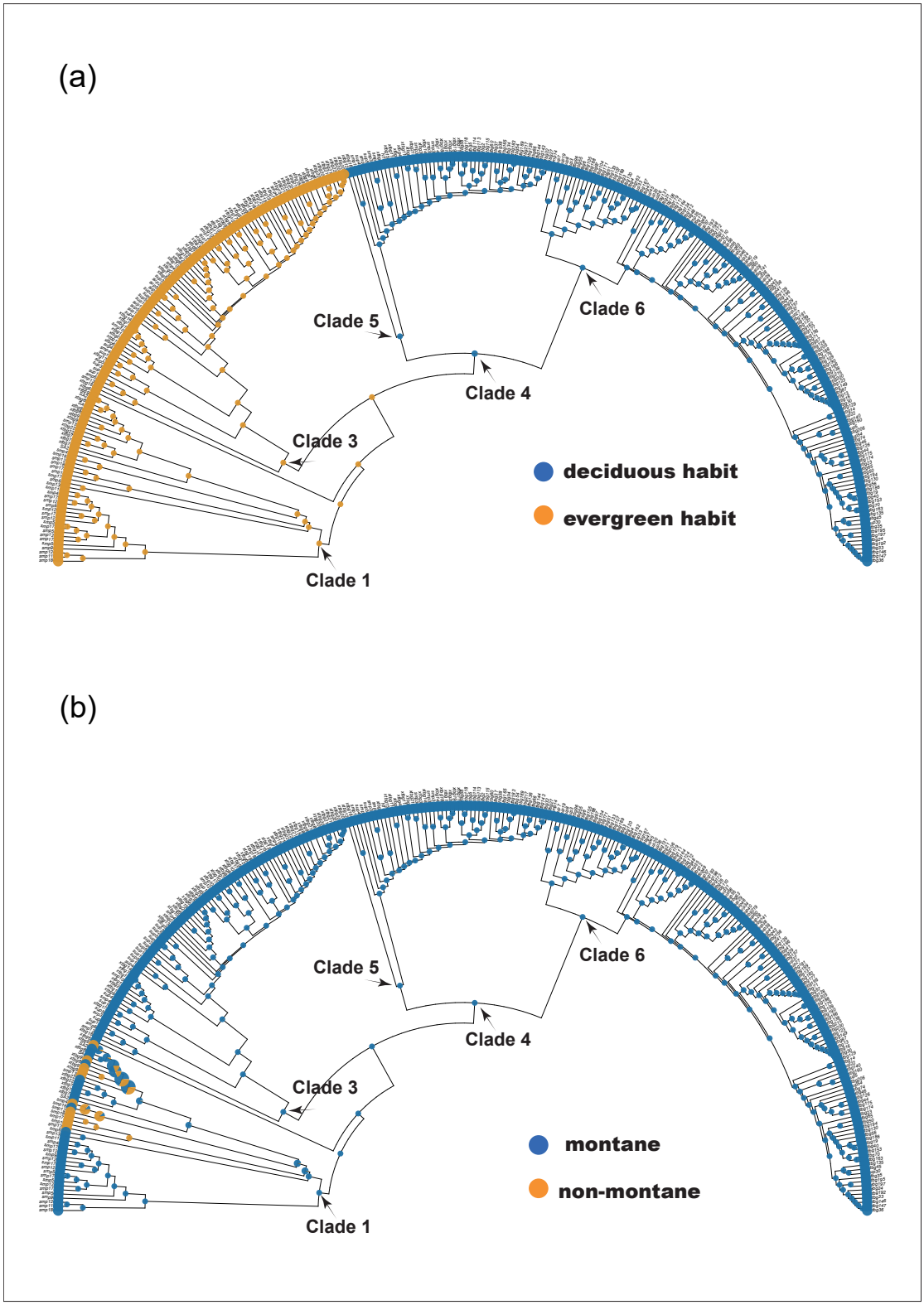


Supplementary Fig. 4. **Ancestral state reconstruction for the selected leaf-traits and habitat type of *Berberis*. a** Deciduousness. **b.** Montane habitat. The pie chart showing the probability of particular state of the common ancestor node, and the major clades of *Berberis* are indicated by the numbers in the colored circles. Source data are provided as a Source Data file.

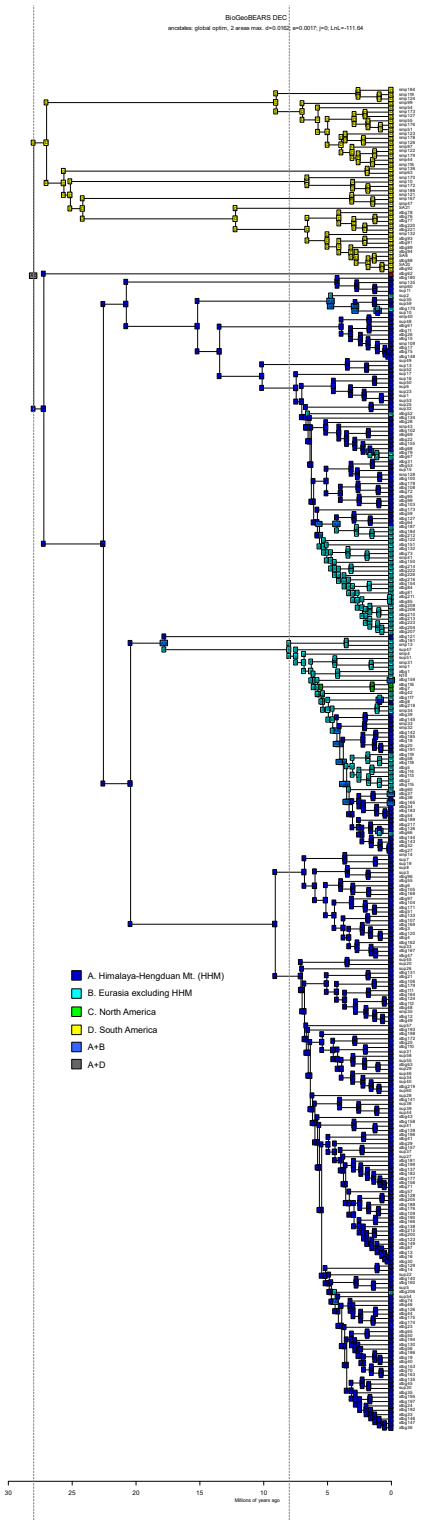


Supplementary Fig. 5. **Ancestral range reconstruction of *Berberis* based on Dispersal-Extinction-Cladogenesis model.** Letters denote the four major biogeographic regions defined in this study: A, Hengduan–Himalaya Mountains (HHM); B, Eurasia excluding the HHM; C, North America; and D, Central and South America. The colored boxes at each node indicate the relative likelihoods of alternative ancestral range combinations, and colored boxes at the tips represent present-day distributions.

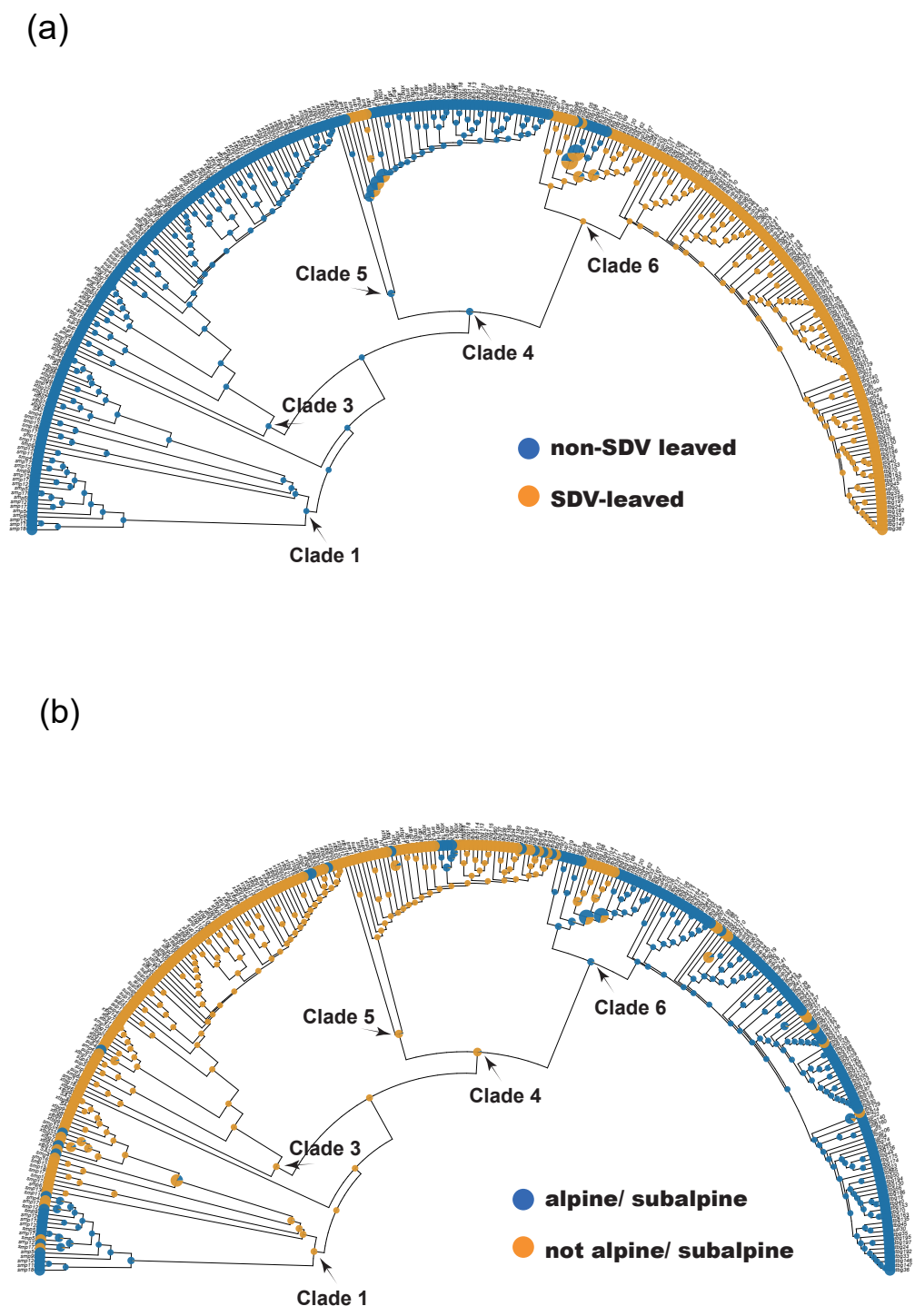


Supplementary Fig. 6. **Ancestral state reconstruction for the selected leaf-traits and habitat type of *Berberis*. a.** small, densely veined leaf. **b.** Alpine/ subalpine habitat. The pie chart showing the probability of particular state of the common ancestor node, and the major clades of *Berberis* are indicated by the numbers in the colored circles. Source data are provided as a Source Data file.

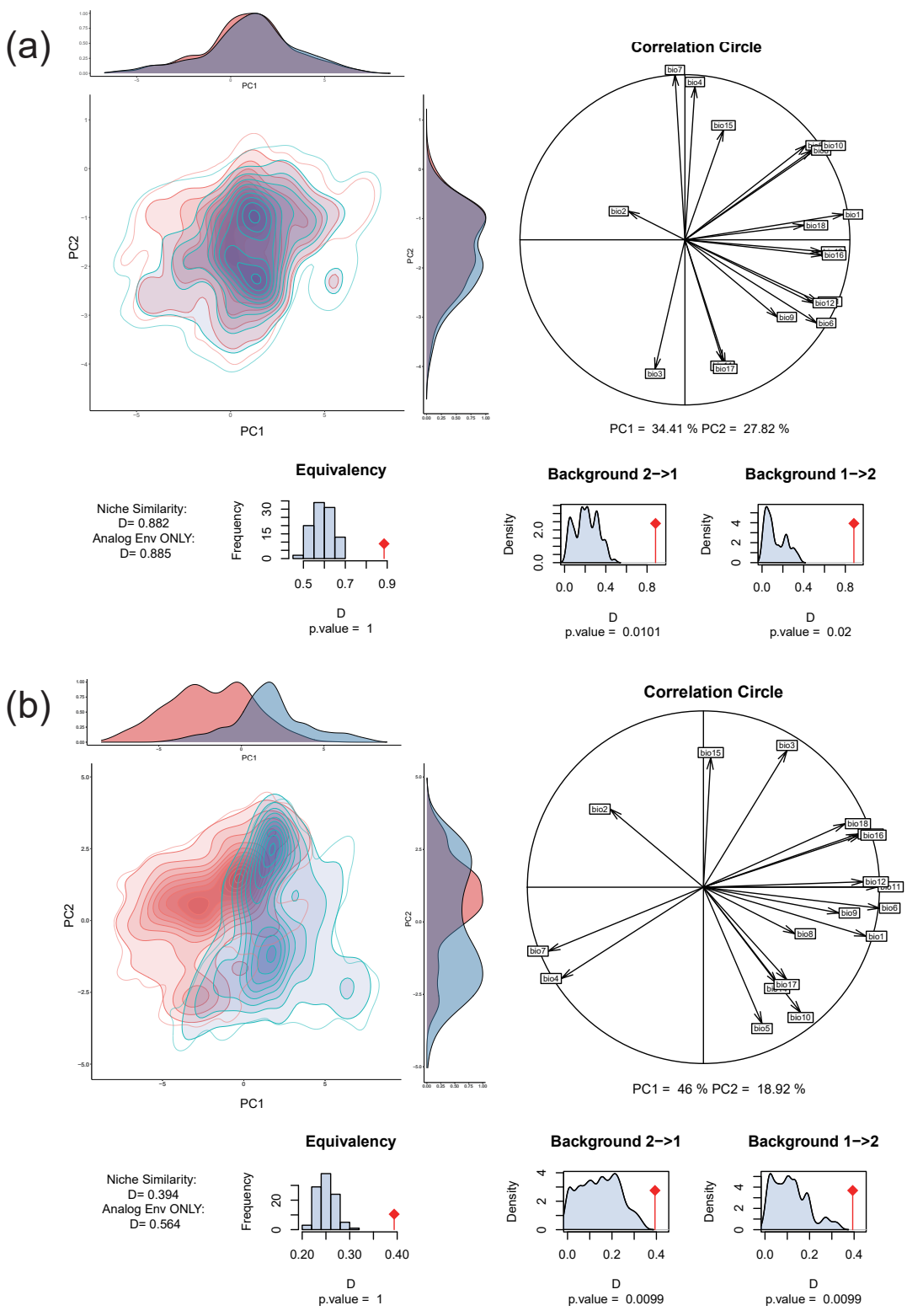


Supplementary Fig. 7. **Climatic niche divergence between the evergreen and deciduous clades of *Berberis*.** For evergreen species, analyses were restricted to endemic taxa to constrain comparisons to lineages associated with montane environments. **a.** Climatic niche comparison between the endemic evergreen *Berberis* species in the Andes (Clade 1) and the Hengduan–Himalaya Mountains (Clade 3-HHMe) based on HUMBOLDT-based principal component analysis (PCA). The two clades occupy broadly overlapping environmental niche space, with partial separation along the first principal component (PC1). The PCA biplot shows the climatic space of Clade 3-HHMe (red) and Clade 1 (blue), with kernel density projections along PC1

and PC2; the percentage of variance explained by each axis is indicated. The correlation circle displays loadings of 19 bioclimatic variables, with variables showing strong contributions (|r| > 0.75) highlighted and used for niche projection. Niche equivalency and similarity tests indicate high climatic niche overlap (Schoener's D = 0.882; analog environment only D = 0.885), and the equivalency test does not reject the null hypothesis of niche identity. Background tests accounting for environmental availability (E-space) show limited niche divergence in both directions (Clade 3-HHMe → Clade 1; Clade 1 → Clade 3-HHMe). **b.** Climatic niche comparison between the endemic evergreen *Berberis* species from the Hengduan–Himalaya Mountains (Clade 3-HHMe) and deciduous non-SDV species (Clade 5) based on HUMBOLDT-based PCA. The two clades show limited overlap in climatic niche space, with pronounced differentiation along the first PC1, which explains the largest proportion of variance. The PCA biplot depicts the climatic space occupied by Clade 5 (red) and Clade 3-HHMe (blue), with kernel density projections along PC1 and PC2; the percentage of variance explained by each axis is indicated. The correlation circle shows loadings of 19 bioclimatic variables, with strongly contributing variables (|r| > 0.75) highlighted and used for niche projection. Niche equivalency and similarity tests indicate moderate overlap (Schoener's D = 0.394; analog environment only D = 0.564), and the equivalency test does not reject niche identity. However, background tests accounting for environmental availability (E-space) detect significant niche divergence in both directions (Clade 5 → Clade 3-HHMe; Clade 3-HHMe → Clade 5, indicating that the two clades occupy distinct portions of the regional climatic landscape.

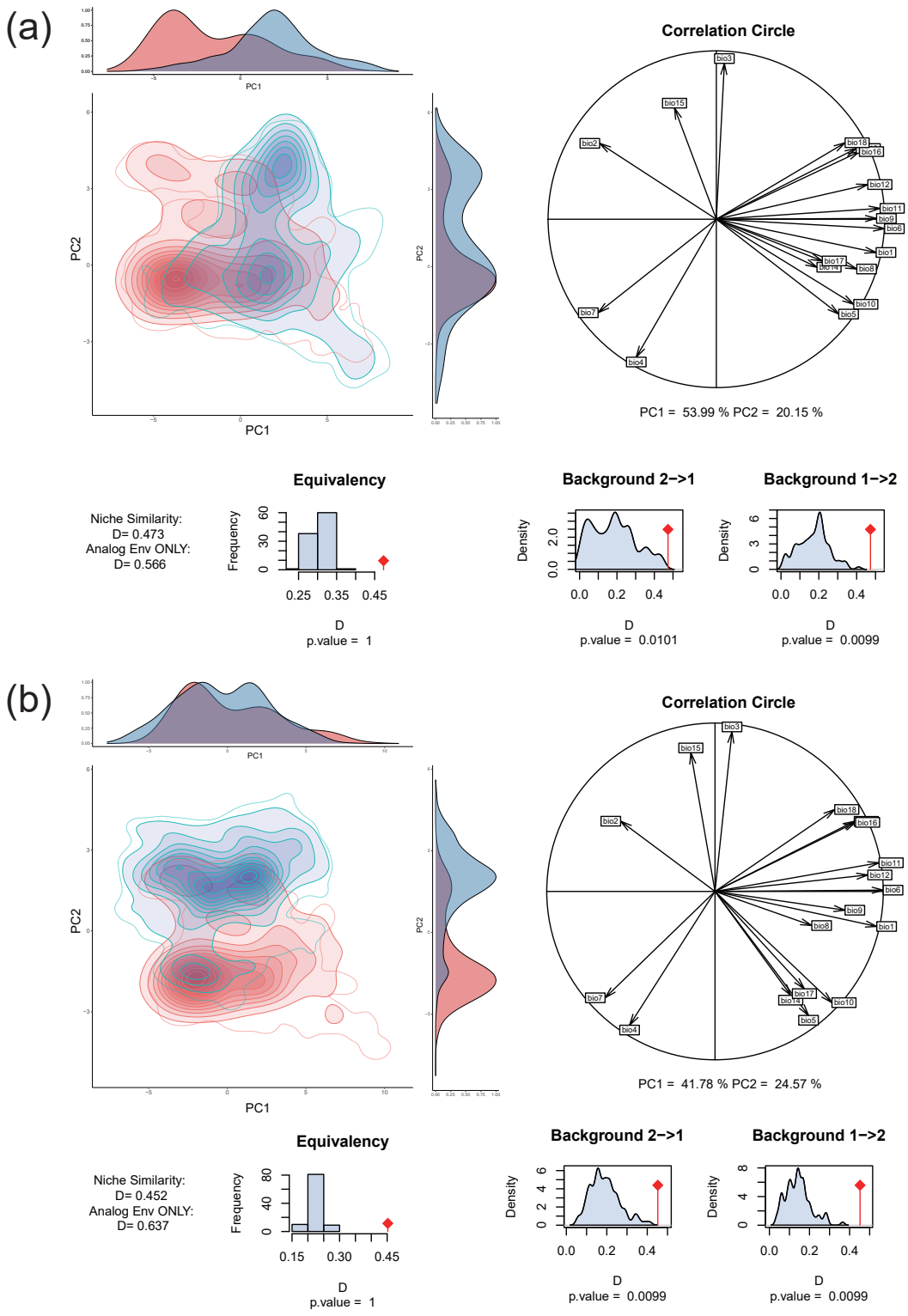


Supplementary Fig. 8. **Climatic niche divergence between the evergreen and deciduous clades of *Berberis*.** For evergreen species, analyses were restricted to endemic taxa to constrain comparisons to lineages associated with montane environments. **a.** Climatic niche comparison between the endemic evergreen *Berberis* species from the Hengduan–Himalaya Mountains (Clade 3-HHMe) and deciduous SDV species (Clade 6) based on HUMBOLDT-based principal component analysis (PCA). The two clades show limited overlap in climatic niche space, with clear differentiation along the first principal component (PC1), which explains the largest proportion of variance. The PCA biplot illustrates the climatic space occupied by Clade

6 (red) and Clade 3-HHMe (blue), with kernel density projections along PC1 and PC2; the proportion of variance explained by each axis is indicated. The correlation circle shows loadings of 19 bioclimatic variables, with strongly contributing variables (|r| > 0.75) highlighted and used for niche projection. Niche equivalency and similarity tests indicate moderate climatic niche overlap (Schoener's D = 0.394; analog environment only D = 0.564), and the equivalency test does not reject niche identity. However, background tests accounting for environmental availability (E-space) detect significant niche divergence in both directions (Clade 6 → Clade 3-HHMe; Clade 3-HHMe → Clade 6), indicating that the two clades occupy distinct portions of the regional climatic landscape. **b.** Climatic niche comparison between the endemic evergreen *Berberis* species from the Hengduan–Himalaya Mountains (Clade 3-HHMe) and deciduous non-SDV species (Clade 5) based on HUMBOLDT-based PCA. The two clades show limited overlap in climatic niche space, with clear differentiation primarily along the PC1, which explains the largest proportion of variance (PC1 = 41.78%, PC2 = 24.57%). The PCA biplot illustrates the climatic space occupied by Clade 5 (red) and Clade 3-HHMe (blue), with kernel density projections along PC1 and PC2; the proportion of variance explained by each axis is indicated. The correlation circle shows loadings of 19 bioclimatic variables, with strongly contributing variables (|r| > 0.75) highlighted and used for niche projection. Niche equivalency and similarity tests indicate moderate climatic niche overlap (Schoener's D = 0.452; analog environment only D = 0.637), and the equivalency test does not reject niche identity. However, background tests accounting for environmental availability (E-space) detect significant niche divergence in both directions (Clade 5 → Clade 3-HHMe; Clade 3-HHMe → Clade 5), indicating that the two clades occupy distinct portions of the regional climatic landscape.

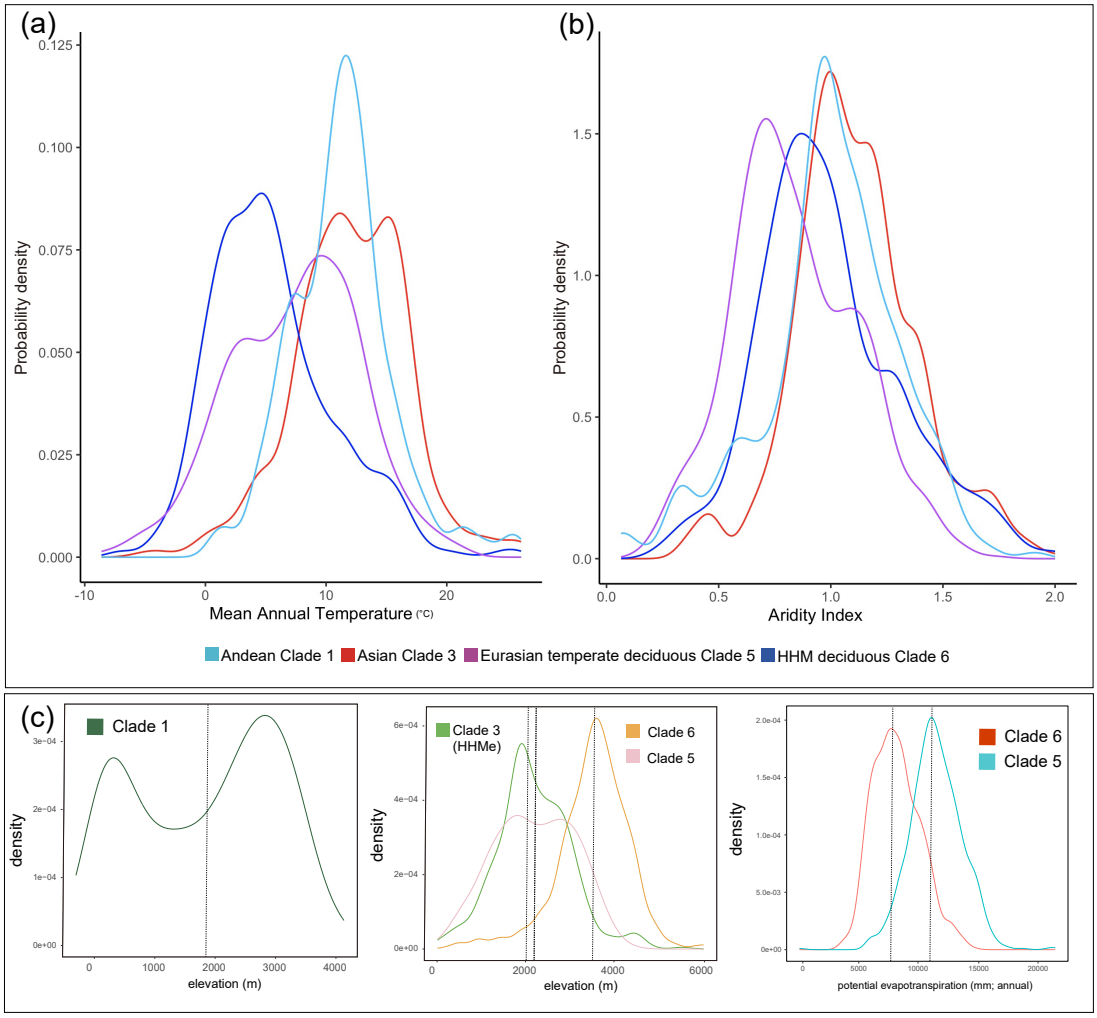


Supplementary Fig. 9. **Probability density functions of climatic variables and elevation for major clades of *Berberis*.** Mean annual temperature (MAT), annual potential evapotranspiration (PET), aridity index (AI), and elevation are shown, with clades indicated by different colors in each panel. MAT was obtained from CHELSA-W5E5 climate data, PET and AI from the Global Aridity Index and Potential Evapotranspiration Database v3, and elevation from WorldClim v2.1. PDFs were calculated from values extracted at species occurrence localities; prior to density estimation, linear trends were removed and PDFs were generated using the R packages ggplot2 and plyr. **a.** Distribution of mean annual temperature (MAT) across major *Berberis* clades. **b.** Distribution of aridity index (AI). **c.** Distribution of elevation, highlighting clade-specific differences in the occupancy of low-, mid-, and high-elevation habitats. Dashed vertical lines indicate the mean elevation for each clade. The left panel shows the distribution for Andean Clade 1, the middle panel for Clades 3-HHMe, 5, and 6, and the right panel shows the distribution of annual potential evapotranspiration (PET), reflecting clade-specific differences in atmospheric water demand. Source data are provided as a Source Data file.

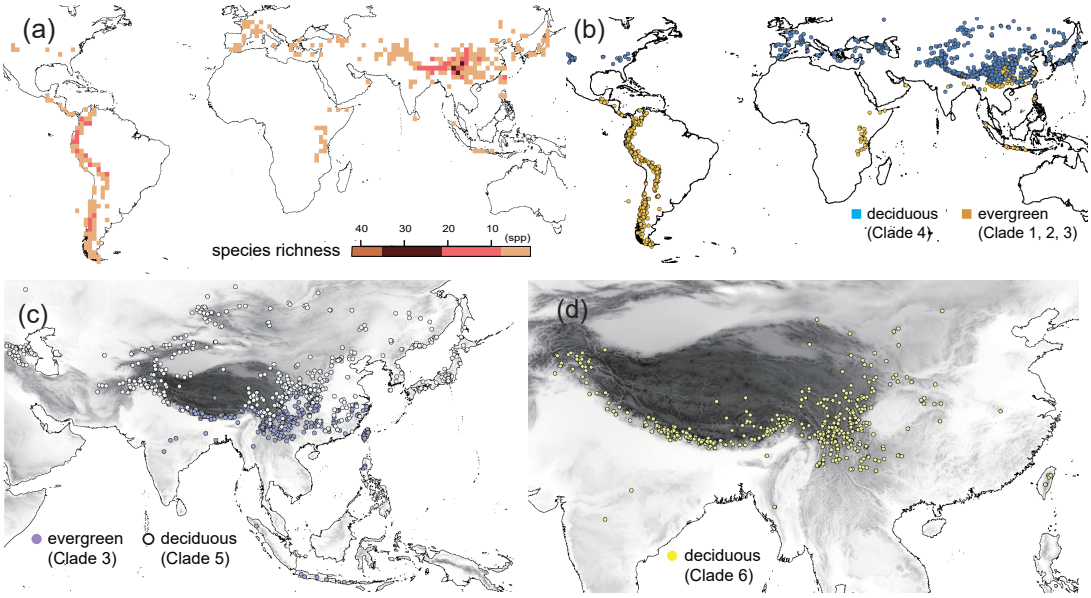


Supplementary Fig. 10. **Global distribution of *Berberis* and geographic ranges of selected clades. a.** Species richness map showing the global distribution of *Berberis* species, with the density of species indicated by a color gradient (10–40 species per grid cell). **b.** Distribution of evergreen (Clades 1–3; yellow) and deciduous (Clade 4; blue) *Berberis* species, highlighting their geographic separation. **c.** Distribution of evergreen (Clade 3; blue) and deciduous (Clade 5; white) *Berberis* species in Eurasia, with species colored by clade. **d.** Distribution of deciduous species from Clade 6 in the Hengduan–Himalaya Mountains, with species locations shown in yellow. In all panels, species are represented as points corresponding to their clade assignments as indicated in the legend. Distribution data are available in the folder “0. Species distribution habitat and sampling” at https://doi.org/10.6084/m9.figshare.28288313

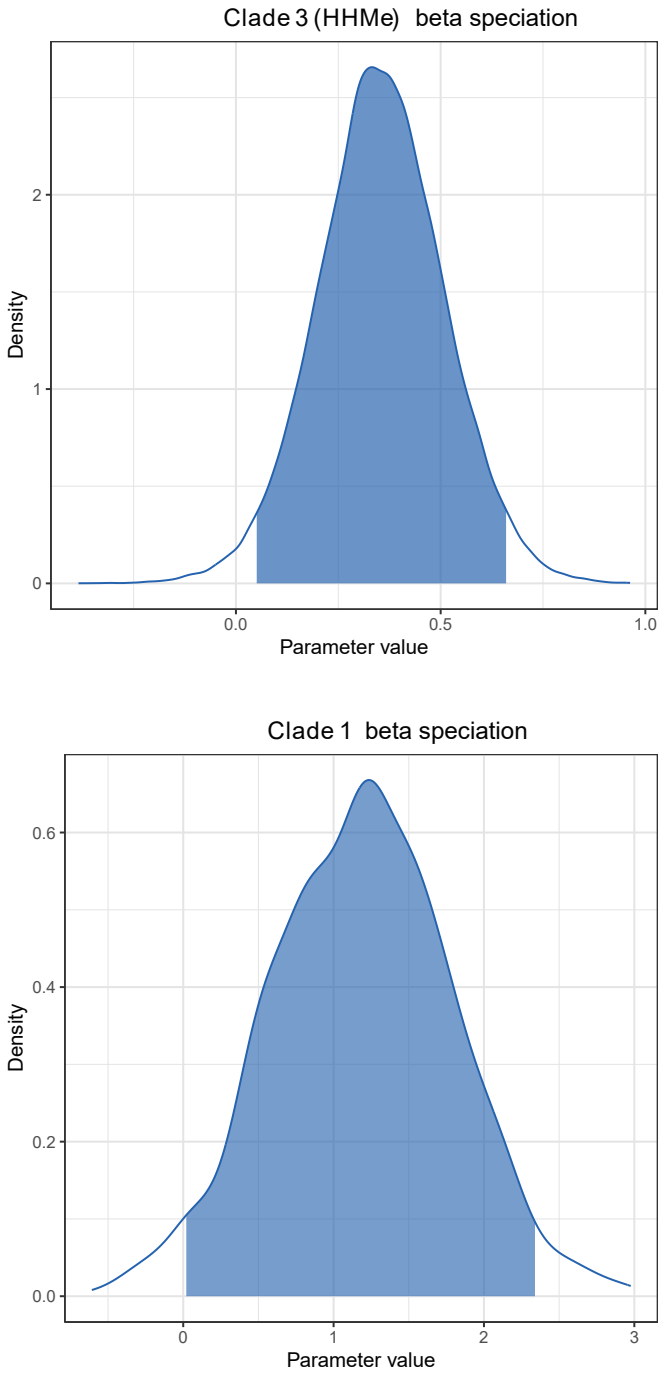


Supplementary Fig. 11. **Posterior distributions of environmental effects on speciation rates.** Posterior density distributions of the speciation parameter ($\beta$ speciation) indicate strong positive correlations between speciation rate and paleotemperature in *Berberis* Clades 1 and 3. Analyses were restricted to endemic taxa from the Andes and the Hengduan–Himalaya Mountains to focus on lineages associated with montane environments. Each distribution was modeled using a reversible-jump mixture prior ($\beta = 0$ or $\beta \sim$ Normal [0, 1]) with equal prior probabilities. The reversible-jump move (mvRJSwitch) allows the chain to sample between the

null model ($\beta = 0$) and the correlation model ($\beta \neq 0$), providing direct posterior estimates of the probability that diversification is environmentally correlated. In both clades, posterior probabilities for $\beta \neq 0$ exceeded 0.9, indicating a strong positive association between speciation rate and paleotemperature change.

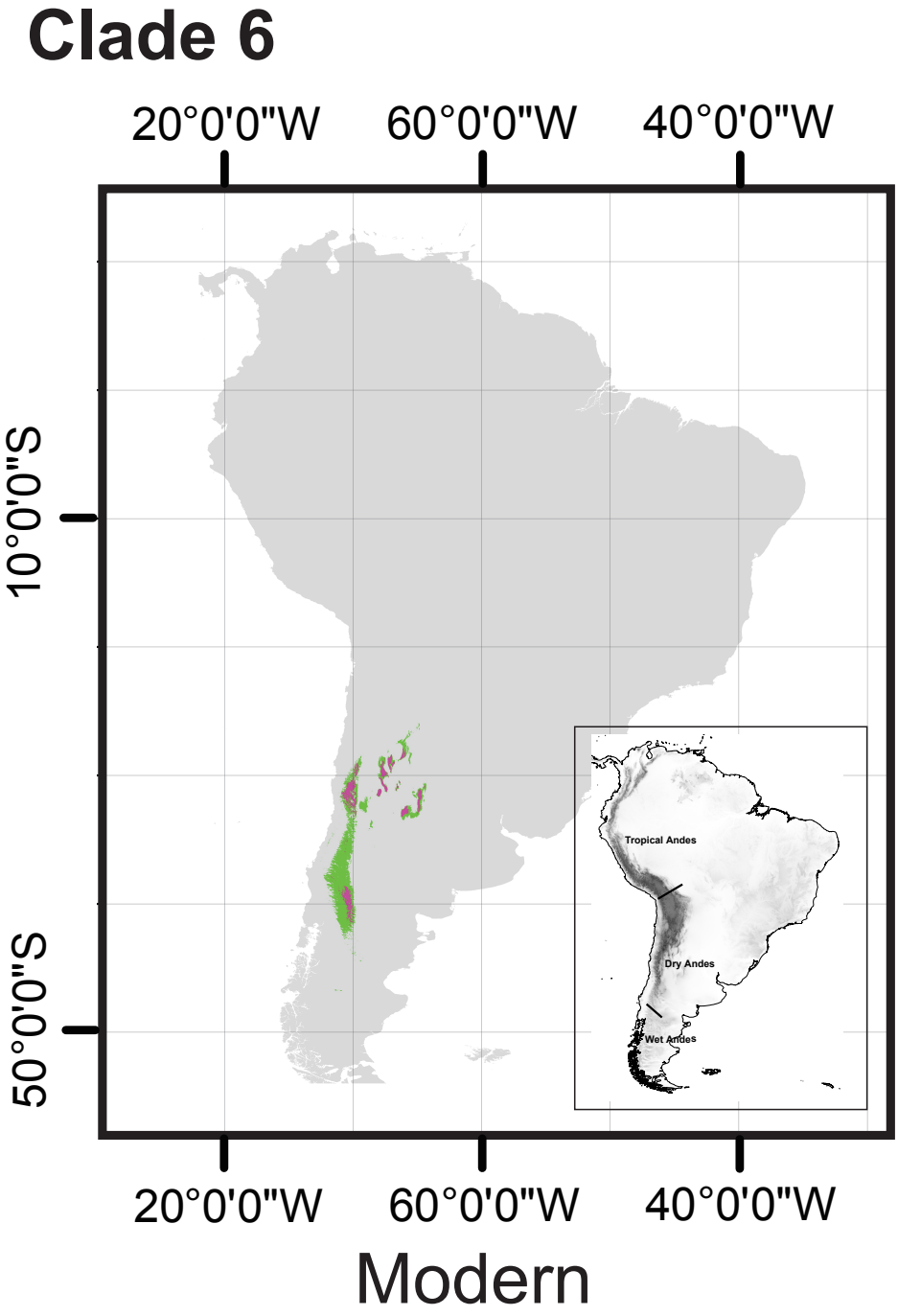


Supplementary Fig. 12. **Potential modern distribution of deciduous Clade 6 in South America.** The potential habitat suitability is shown as moderate suitability (0.4–0.7, green) and high suitability (0.7–0.9, reddish pink). The inset map shows the major Andean biogeographic regions, with the Tropical Andes, Dry Andes, and Wet Andes indicated.

Supplementary Table 1. **Mechanistic links between leaf morphological traits and hydraulic strategies as drivers of fitness in high-elevation environments.**

| Leaf trait | Explanation | Case studies and lines of evidence |
|---|---|---|
| Small leaf size | Plants evolving smaller leaves reduce boundary-layer thickness, better dissipate heat under strong solar radiation, shorten internal water-transport distances, and compartmentalize hydraulic risk (e.g., from freeze–thaw or embolism). In alpine environments, small leaves may facilitate rapid rehydration, minimize overheating, and reduce mechanical damage from wind or cold. | 1. Recent macroecological analyses indicate that leaf size represents an additional functional axis associated with cold tolerance, independent of the classical leaf-economics spectrum. In alpine floras, this "cold-tolerance dimension" reflects an adaptive coordination between leaf morphology and thermal regulation, whereby smaller leaves enhance heat dissipation, reduce frost damage, and maintain hydraulic integrity under low-temperature and high-radiation conditions (16). |
| High major vein length per area | The hydraulic efficiency-safety trade-off drives high mountain plants towards robust, safety-oriented vein architectures, including increased main vein density, to maintain stable water function despite high diurnal vapor pressure deficit vapor pressure deficit and freeze-thaw stress prevailing in the alpine environment.<br><br>High major vein density also provides biomechanical support, which would enhance structural integrity helps leaves resist high wind stress in alpine environment. | 1. The increased major vein density is hypothesized to compensate for the short growing season by supporting high photosynthetic and stomatal capacity, thereby overcoming the constraints of high diurnal vapor pressure deficit and freeze-thaw stress prevailing in the alpine environment (17).<br><br>2. The high investment in major vein density serves as a critical anatomical basis for high-elevation shrubs to enhance hydraulic safety, often reflected by an increase in the ratio of major to minor vein densities. This structural fortification is essential for maintaining the integrity of the leaf water transport system against the severe environmental constraints of high altitudes, including low temperature, low atmospheric pressure, and potential water stress (18). |

| | | |
|---|---|---|
| | | 3. High major vein density leaves show lower vulnerability to freeze–thaw embolism due to network redundancy (18).<br><br>4. When subjected to shear and tearing forces from strong winds, dense vein network effectively disperses the pressure across the entire leaf, thereby preventing localized damage and maintaining overall structural integrity (18, 19). |
| Deciduous habit | Deciduous habit is tightly linked to temperature decline and seasonality. Evergreen species typically exhibit conservative leaf-economics strategies, high leaf mass per area and long leaf lifespan, that enable sustained carbon gain under resource scarcity. In contrast, deciduous species adopt a “rapid acquisition–rapid turnover” strategy: their leaves are more acquisitive, achieving high photosynthetic returns during short warm periods, then reabsorbing nutrients (N, P) before leaf senescence to avoid freeze damage. Leaf shedding is a strategy against winter embolism and cold-induced dehydration (“physiological drought”), allowing species to survive severe frost and nutrient-poor soils. | 1. Deciduous species in high-elevation ecosystems exhibit a short Leaf Lifespan and a high Nitrogen content, representing a "fast-return" resource-acquisition strategy that is functionally distinct from the "slow-return" strategy of evergreen species (8, 20).<br><br>2. At higher elevations, deciduous and evergreen species exhibit greater functional divergence, indicating that the deciduous habit represents a distinct adaptive trajectory that accelerates lineage differentiation in functional trait space. This pattern suggests that elevation promotes coordinated divergence between phylogeny and function by favoring contrasting ecological strategies under increasing environmental stress (e.g. 20, 21). |

Supplementary Table 2. **Species diversity of *Berberis* across the Andes and the Hengduan-Himalaya Mts. (HHM).**

| | Andes | Hengduan- Himalaya Mts. | Total |
|---|---|---|---|
| Evergreen | 42/90 (ca. 47%) | 52/71 (ca. 73%) | 94/161 (ca. 58%) |
| Deciduous | 0 | 140/186 (ca. 75%) | 122/186 (ca. 66%) |
| Total | 42/90 (ca. 47%) | 192/257 (ca. 75%) | 216/347 (ca. 62%) |
| Numbers in the left indicate taxa sampled in this study. | | | |

Supplementary Table 3. **Trait state investigated in both the Multistate hidden Speciation and Extinction (MuHiSSE) & Multistate Speciation and Extinction (MuSSE) models.**

| Trait | Scenario | State |
|---|---|---|
| Leaf habit (LH): | 1 | Evergreen (coded as 0) vs<br>Deciduous (coded as 1) |
| | 2 | non SDV deciduous leaf (coded as 0) vs<br>SDV deciduous leaf (coded as 1) |
| Habitat type (HT): | 1 | non montane (coded as 0) vs<br>montane (coded as 1) |
| | 2 | non high-elevation (coded as 0) vs<br>high-elevation (coded as 1) |
| The small, densely leaf was in abbreviation as 'SDV leaf'. See Methods for detailed description of Scenario 1 & 2. | | |

Supplementary Table 4. **Parameterization and biological interpretation of candidate MuHiSSE models evaluated in this study.**

| model | model_class | hidden_classes | assumptions |
|---|---|---|---|
| MuSSE-like_null | MuSSE-like | 0 | No hidden states; turnover and eps constrained equal across observed states. |
| MuSSE-like_turnover-only | MuSSE-like | 0 | No hidden states; turnover varies among observed states; eps constrained equal. |
| MuSSE-like_full | MuSSE-like | 0 | No hidden states; turnover and eps both vary among observed states. |
| MuHiSSE_trait-dependent_full01 | MuHiSSE trait-dependent | 2 | Two hidden classes; turnover varies across observed and hidden states; eps constrained equal. |
| MuHiSSE_trait-dependent_full02 | MuHiSSE trait-dependent | 3 | Three hidden classes; turnover and eps vary across observed and hidden states. |
| CID2_hidden_2_classes | CID | 2 | Character-independent diversification model with two hidden classes; observed states do not directly affect diversification. |
| CID4_hidden_4_classes | CID | 4 | Character-independent diversification model with four hidden classes; observed states do not directly affect diversification. |
| CID5_hidden_5_classes | CID | 5 | Character-independent diversification model with five hidden classes; observed states do not directly affect diversification. |

Supplementary Table 5. **Parameterization of representative MuHiSSE models showing state-dependent transition constraints and diversification parameters.**

MuSSE-like null model (no hidden states), in which turnover and extinction fraction are constrained to be equal across all observed states.
Turnover rate: (1,1,1,1) / Extinction fraction: (1,1,1,1)

| | LH(0)-HT(0) | LH(0)-HT(1) | LH(1)-HT(0) | LH(1)-HT(1) | | | | |
|---|---|---|---|---|---|---|---|---|
| LH(0)-HT(0) | NA | 3 | 5 | NA | | | | |
| LH(0)-HT(1) | 1 | NA | 0 | 7 | | | | |
| LH(1)-HT(0) | 2 | 0 | NA | 8 | | | | |
| LH(1)-HT(1) | NA | 4 | 6 | NA | | | | |

MuSSE-like turnover-only model (no hidden states), in which turnover varies among observed states while extinction fraction is constrained to be equal.
Turnover rate: (1,2,3,4) / Extinction fraction: (1,1,1,1)

| | LH(0)-HT(0) | LH(0)-HT(1) | LH(1)-HT(0) | LH(1)-HT(1) | | | | |
|---|---|---|---|---|---|---|---|---|
| LH(0)-HT(0) | NA | 3 | 5 | NA | | | | |
| LH(0)-HT(1) | 1 | NA | 0 | 7 | | | | |
| LH(1)-HT(0) | 2 | 0 | NA | 8 | | | | |
| LH(1)-HT(1) | NA | 4 | 6 | NA | | | | |

MuHiSSE trait-dependent model with two hidden classes (A and B), in which turnover varies across observed and hidden states, while extinction fraction is constrained to be equal.
Turnover rate: (1,2,3,4,5,6,7,8) / Extinction fraction: (1,1,1,1,1,1,1,1)

| | LH(0)-HT(0) /A | LH(0)-HT(1) /A | LH(1)-HT(0) /A | LH(1)-HT(1) /A | LH(0)-HT(0) /B | LH(0)-HT(1) /B | LH(1)-HT(0) /B | LH(1)-HT(1)/B |
|---|---|---|---|---|---|---|---|---|
| LH(0)-HT(0) /A | NA | 3 | 5 | NA | 17 | NA | NA | NA |
| LH(0)-HT(1) /A | 1 | NA | 0 | 7 | NA | 17 | NA | NA |
| LH(1)-HT(0) /A | 2 | 0 | NA | 8 | NA | NA | 17 | NA |
| LH(1)-HT(1) /A | 0 | 4 | 6 | NA | NA | NA | NA | 17 |
| LH(0)-HT(0) /B | 17 | NA | NA | NA | NA | 11 | 13 | NA |
| LH(0)-HT(1) /B | NA | 17 | NA | NA | 9 | NA | 0 | 15 |
| LH(1)-HT(0) /B | NA | NA | 17 | NA | 10 | 0 | NA | 16 |
| LH(1)-HT(1)/ B | NA | NA | NA | 17 | NA | 12 | 14 | NA |

MuHiSSE trait-dependent model with two hidden classes (A and B), in which turnover varies across observed and hidden states, while extinction fraction is constrained to be equal.
Turnover rate: (1,2,3,4,5,6,7,8) / Extinction fraction: (1,1,1,1,1,1,1,1)

| | LH(0)-HT(0) /A | LH(0)-HT(1) /A | LH(1)-HT(0) /A | LH(1)-HT(1) /A | LH(0)-HT(0) /B | LH(0)-HT(1) /B | LH(1)-HT(0) /B | LH(1)-HT(1)/B |
|---|---|---|---|---|---|---|---|---|
| LH(0)-HT(0) /A | NA | 3 | 5 | NA | 17 | NA | NA | NA |
| LH(0)-HT(1) /A | 1 | NA | 0 | 7 | NA | 17 | NA | NA |
| LH(1)-HT(0) /A | 2 | 0 | NA | 8 | NA | NA | 17 | NA |
| LH(1)-HT(1) /A | 0 | 4 | 6 | NA | NA | NA | NA | 17 |
| LH(0)-HT(0) /B | 17 | NA | NA | NA | NA | 11 | 13 | NA |
| LH(0)-HT(1) /B | NA | 17 | NA | NA | 9 | NA | 0 | 15 |
| LH(1)-HT(0) /B | NA | NA | 17 | NA | 10 | 0 | NA | 16 |
| LH(1)-HT(1)/ B | NA | NA | NA | 17 | NA | 12 | 14 | NA |

Character-independent diversification (CID) model with two hidden classes, in which diversification rates vary across hidden states but are independent of observed traits.
Turnover rate: (1,1,1,1,2,2,2,2) / Extinction fraction: (1,1,1,1,2,2,2,2)

| | LH(0)-HT(0) /A | LH(0)-HT(1) /A | LH(1)-HT(0) /A | LH(1)-HT(1) /A | LH(0)-HT(0) /B | LH(0)-HT(1) /B | LH(1)-HT(0) /B | LH(1)-HT(1) /B |
|---|---|---|---|---|---|---|---|---|
| LH(0)-HT(0) /A | NA | 3 | 5 | 0 | 9 | NA | NA | NA |
| LH(0)-HT(1) /A | 1 | NA | 0 | 7 | NA | 9 | NA | NA |
| LH(1)-HT(0) /A | 2 | 0 | NA | 8 | NA | NA | 9 | NA |
| LH(1)-HT(1) /A | 0 | 4 | 6 | NA | NA | NA | NA | 9 |
| LH(0)-HT(0) /B | 33 | NA | NA | NA | NA | 10 | 12 | NA |

| | | | | | | | | |
|---|---|---|---|---|---|---|---|---|
| LH(0)-HT(1) /B | NA | 33 | NA | NA | 11 | NA | 0 | 14 |
| LH(1)-HT(0) /B | NA | NA | 33 | NA | 13 | 0 | NA | 16 |
| LH(1)-HT(1)/B | NA | NA | NA | NA | 0 | 16 | 17 | NA |

CID model with increased hidden-state complexity (four to five hidden classes), in which diversification rates vary across hidden states independent of observed traits.
CID4: Turnover rate = (1,1,1,1,2,2,2,2,3,3,3,3,4,4,4,4); extinction fraction = (1,1,1,1,2,2,2,2,3,3,3,3,4,4,4,4)
CID5: Turnover rate = (1,1,1,1,2,2,2,2,3,3,3,3,4,4,4,4,5,5,5,5); extinction fraction = (1,1,1,1,2,2,2,2,3,3,3,3,4,4,4,4,5,5,5,5)

| | LH(0)-HT(0) /A | LH(0)-HT(1) /A | LH(1)-HT(0) /A | LH(1)-HT(1) /A | X2-7 | LH(0)-HT(0) /B | LH(0)-HT(1) /B | LH(1)-HT(0) /B |
|---|---|---|---|---|---|---|---|---|
| LH(0)-HT(0) /A | NA | 3 | 5 | 0 | … | 65 | NA | NA |
| LH(0)-HT(1) /A | 1 | NA | 0 | 7 | … | NA | 65 | NA |
| LH(1)-HT(0) /A | 2 | 0 | NA | 8 | … | NA | NA | 65 |
| LH(1)-HT(1) /A | 0 | 4 | 6 | NA | … | NA | NA | NA |
| X2-7 | … | … | … | … | … | … | … | … |
| LH(0)-HT(0) /B | 65 | NA | NA | NA | … | NA | 59 | 61 |
| LH(0)-HT(1) /B | NA | 65 | NA | NA | … | 57 | NA | 0 |
| LH(1)-HT(0) /B | NA | NA | 65 | NA | … | 58 | 0 | NA |
| LH(1)-HT(1) /B | NA | NA | NA | 65 | … | 0 | 60 | 62 |

This table summarizes the parameterization of representative MuHiSSE models used in the analyses. Each matrix defines allowed transitions among combined states of leaf habit (LH), habitat type (HT), and hidden classes (A and B). Cells contain indices of transition-rate parameters (q_ij), with identical numbers indicating shared parameters across transitions.

Simultaneous transitions between both observed traits (i.e., dual transitions such as 00 → 11 or 11 → 00) were disallowed and are indicated as “NA”. This constraint reflects the biological expectation that, in *Berberis*, shifts in leaf habit and habitat preference are unlikely to occur simultaneously, as these traits are associated with distinct ecological and physiological adaptations. In addition, disallowing dual transitions reduces model complexity and improves parameter identifiability.

Turnover (τ = speciation + extinction) and extinction fraction (ε = extinction / speciation) parameters are listed below each matrix, with shared values indicating constraints across states. Model differences reflect alternative assumptions about whether diversification rates vary among observed states, hidden states, or both.

For clarity, only six representative models are shown. Two additional candidate models (a MuSSE-like model with alternative parameter constraints and a CID model with an intermediate number of hidden classes) were evaluated but are not shown, as they represent intermediate parameterizations within the same model families and do not introduce qualitatively different biological hypotheses.

Abbreviations: LH, leaf habit; HT, habitat type. State definitions follow those described in the main text.

Supplementary Table 6. **Model comparison of candidate state-dependent diversification models inferred using MuHiSSE for each focal trait combination in *Berberis* (Scenario 1).**

| model | logLik | k | AIC | AICc | delta_AICc | weight |
|---|---|---|---|---|---|---|
| MuSSE-like_turnover-only | -704.652 | 13 | 1461.303 | 1466.317 | 0 | 0.5197 |
| CID2_hidden_2_classes | -710.548 | 21 | 1463.096 | 1471.338 | 5.021 | 0.4746 |
| MuHiSSE_trait-dependent_full01 | -724.102 | 26 | 1474.204 | 1475.446 | 4.108 | 0.0052 |
| MuSSE-like_full | -723.086 | 16 | 1478.173 | 1480.049 | 13.731 | 5.00E-04 |
| MuSSE-like_null | -741.22 | 10 | 1502.441 | 1503.184 | 36.867 | 0 |
| CID4_hidden_4_classes | -707.227 | 41 | 1496.454 | 1509.45 | 43.133 | 0 |
| MuHiSSE_trait-dependent_full02 | -699.723 | 49 | 1497.447 | 1516.513 | 50.196 | 0 |
| CID5_hidden_5_classes | -698.713 | 51 | 1499.427 | 1520.227 | 53.909 | 0 |

Candidate models were ranked by Akaike's Information Criterion corrected for small sample size (AICc). The table reports the number of free parameters (k), maximized log-likelihood (lnL), AICc, ΔAICc relative to the best-supported model, and Akaike weight (wi). MuSSE models evaluate diversification-rate variation directly associated with observed trait states, whereas MuHiSSE models additionally incorporate hidden states to account for unmeasured diversification-rate heterogeneity. CID models are character-independent diversification models in which diversification-rate variation is associated with hidden states rather than the focal observed traits. Lower AICc values indicate stronger relative support.

Supplementary Table 7. **Model comparison of candidate state-dependent diversification models inferred using MuHiSSE for each focal trait combination in *Berberis* (Scenario 2).**

| model | logLik | k | AIC | AICc | delta_AICc | weight |
|---|---|---|---|---|---|---|
| MuSSE-like_turnover-only | -409.032 | 13 | 844.063 | 846.31 | 0 | 0.9948 |
| CID2_hidden_2_classes | -405.08 | 21 | 852.16 | 858.16 | 11.849 | 0.0027 |
| MuSSE-like_full | -411.637 | 16 | 855.275 | 858.696 | 12.386 | 0.002 |
| MuSSE-like_null | -420.505 | 10 | 861.009 | 862.343 | 16.032 | 3.00E-04 |
| MuHiSSE_trait-dependent_full01 | -400.912 | 26 | 853.824 | 863.247 | 16.936 | 2.00E-04 |
| CID4_hidden_4_classes | -397.814 | 41 | 877.628 | 903.329 | 57.019 | 0 |
| MuHiSSE_trait-dependent_full02 | -395.931 | 49 | 889.862 | 928.751 | 82.441 | 0 |
| CID5_hidden_5_classes | -399.267 | 51 | 900.534 | 943.308 | 96.998 | 0 |

Supplementary Table 8. **Parameterization and biological interpretation of candidate MuSSE models evaluated in this study.**

| Model | λ parameters | μ parameters | q parameters | Biological meaning |
|---|---|---|---|---|
| Null | λ00 = λ10 = λ01 = λ11 | μ00 = μ10 = μ01 = μ11 | $q_{ij}$ free | No trait effect on diversification |
| λ additive | λ00, λ10, λ01, λ11 via additive effects | μ equal | $q_{ij}$ free | Independent effects of deciduousness and montane state on speciation |
| λ interaction | λ11 includes interaction term | μ equal | $q_{ij}$ free | Synergistic effect when both traits co-occur |
| λ + μ additive | λ additive; μ additive | state dependent | $q_{ij}$ free | Traits affect both speciation and extinction |
| Full additive | λ, μ, q all trait-dependent | state dependent | state dependent | Fully trait-dependent diversification model |

Supplementary Table 9. **Parameterization and assumptions of candidate MuSSE models used to evaluate trait-dependent diversification.**

| model | depth | assumptions |
|---|---|---|
| M0_null_no_trait_effect | depth = 0 | Trait transition rates vary, but speciation and extinction are not trait-dependent. |
| M1_lambda_additive | depth = c(1,0,0) | Speciation varies additively with the two traits; extinction and transition rates are not trait-dependent. |
| M2_mu_additive | depth = c(0,1,0) | Extinction varies additively with the two traits; speciation and transition rates are not trait-dependent. |
| M3_q_additive | depth = c(0,0,1) | Transition rates vary additively with the two traits; speciation and extinction are not trait-dependent. |
| M4_lambda_mu_additive | depth = c(1,1,0) | Speciation and extinction vary additively with the two traits; transition rates are not trait-dependent. |
| M5_lambda_mu_q_additive | depth = c(1,1,1) | Speciation, extinction, and transition rates all vary additively with the two traits. |
| M6_lambda_interaction | depth = c(2,0,0) | Speciation includes an interaction between the two traits; extinction and transition rates are not trait-dependent. |
| M7_mu_interaction | depth = c(0,2,0) | Extinction includes an interaction between the two traits; speciation and transition rates are not trait-dependent. |
| M8_lambda_mu_interaction | depth = c(2,2,0) | Speciation and extinction include interactions between the two traits; transition rates are not trait-dependent. |

Supplementary Table 10. **Model comparison of candidate MuSSE models under Scenario 1 using an AICc-based framework.**

| model | logLik | k | AIC | AICc | delta_AICc | weight |
|---|---|---|---|---|---|---|
| M6_lambda_interaction | -721.66 | 9 | 1461.319 | 1461.925 | 0 | 0.6362 |
| M1_lambda | -723.419 | 8 | 1462.838 | 1463.321 | 1.396 | 0.3166 |
| M4_lambda_mu | -723.395 | 10 | 1466.79 | 1467.533 | 5.608 | 0.0385 |
| M2_mu | -727.089 | 8 | 1470.177 | 1470.66 | 8.735 | 0.0081 |
| M8_lambda_mu_interaction | -725.896 | 12 | 1475.791 | 1476.852 | 14.927 | 4.00E-04 |
| M5_full_additive | -724.381 | 14 | 1476.762 | 1478.201 | 16.276 | 2.00E-04 |
| M7_mu_interaction | -733.805 | 9 | 1485.609 | 1486.215 | 24.29 | 0 |
| M0_null | -741.542 | 6 | 1495.085 | 1495.365 | 33.44 | 0 |

Supplementary Table 11. **Model comparison of candidate MuSSE models under Scenario 2 using an AICc-based framework.**

| model | logLik | k | AIC | AICc | delta_AICc | weight |
|---|---|---|---|---|---|---|
| M1_lambda_additive | -419.146 | 8 | 854.292 | 855.154 | 0 | 0.5885 |
| M6_lambda_interaction | -419.049 | 9 | 856.099 | 857.183 | 2.029 | 0.2133 |
| M5_lambda_mu_q_additive | -413.859 | 14 | 855.717 | 858.326 | 3.172 | 0.1205 |
| M4_lambda_mu_additive | -419.127 | 10 | 858.253 | 859.587 | 4.433 | 0.0641 |
| M2_mu_additive | -423.098 | 8 | 862.195 | 863.058 | 7.904 | 0.0113 |
| M0_null_no_trait_effect | -427.385 | 6 | 866.77 | 867.267 | 12.113 | 0.0014 |
| M3_q_additive | -423.464 | 10 | 866.927 | 868.26 | 13.106 | 8.00E-04 |
| M7_mu_interaction | -733.805 | 9 | 1485.609 | 1486.215 | 24.29 | 0 |

Supplementary Table 12. **Pairwise comparisons of state-specific speciation rates among trait–habitat combinations shown in Fig. 2c.** Results of two-sided pairwise Welch t-tests comparing tree-level mean state-specific speciation-rate estimates across 100 sampled phylogenies. Reported values include the test statistic (t), degrees of freedom (df), *p* value, mean difference, Cohen's d effect size, and 95% confidence intervals.

| comparison | statistic | t value | df | *p* value | CI lower | CI upper | Mean difference |
|---|---|---|---|---|---|---|---|
| λ00: non-deciduous, non-montane vs λ10: deciduous, non-montane | Welch two-sample t-test | -11.761004 | 191.384289 | <2.2e-16 | -0.0415238 | -0.0295963 | -0.0355601 |
| λ00: non-deciduous, non-montane vs λ01: non-deciduous, montane | Welch two-sample t-test | -79.685106 | 194.886592 | <2.2e-16 | -0.238335 | -0.2268224 | -0.2325787 |
| λ10: deciduous, non-montane vs λ11: deciduous, montane | Welch two-sample t-test | -74.728988 | 195.223324 | <2.2e-16 | -0.2387167 | -0.2264407 | -0.2325787 |
| λ01: non-deciduous, montane vs λ11: deciduous, montane | Welch two-sample t-test | -11.8118 | 197.319514 | <2.2e-16 | -0.041497 | -0.0296231 | -0.0355601 |
| **comparison** | **statistic** | **Effect size** | **CI lower** | **CI upper** | **N. of group1** | **N. of group2** | |
| λ00: non-deciduous, non-montane vs λ10: deciduous, non-montane | Cohen's d | -1.6632572 | -1.9835914 | -1.3397571 | 100 | 100 | |
| λ00: non-deciduous, non-montane vs λ01: non-deciduous, montane | Cohen's d | -11.269176 | -12.398956 | -10.110938 | 100 | 100 | |
| λ10: deciduous, non-montane vs λ11: deciduous, montane | Cohen's d | -10.568275 | -11.632094 | -9.4777681 | 100 | 100 | |
| λ01: non-deciduous, montane vs λ11: deciduous, montane | Cohen's d | -1.6704408 | -1.9911316 | -1.346577 | 100 | 100 | |

Supplementary Table 13. **Pairwise comparisons of state-specific speciation rates among trait–habitat combinations shown in Fig. 2d.** Results of two-sided pairwise Welch t-tests comparing tree-level mean state-specific speciation-rate estimates across 100 sampled phylogenies. Reported values include the test statistic (t), degrees of freedom (df), *p* value, mean difference, Cohen's d effect size, and 95% confidence intervals.

| comparison | statistic | t value | df | *p* value | CI lower | CI upper | Mean difference |
|---|---|---|---|---|---|---|---|
| λ00: non-SDV, non high-elevation vs λ10: deciduous SDV leaves, non high-elevation | Welch two-sample t-test | -20.529483 | 197.96706 | <2.2e-16 | -0.0596523 | -0.0491965 | -0.0544244 |
| λ00: non-SDV, non high-elevation vs λ01: non deciduous SDV leaves, high-elevation | Welch two-sample t-test | -11.499845 | 197.999713 | <2.2e-16 | -0.0355047 | -0.0251103 | -0.0303075 |
| λ10: deciduous SDV leaves, non high-elevation vs λ11: deciduous SDV leaves, high-elevation | Welch two-sample t-test | -28.368097 | 186.932725 | <2.2e-16 | -0.0930616 | -0.08096 | -0.0870108 |

| | | | | | | | |
|---|---|---|---|---|---|---|---|
| λ01: non deciduous SDV leaves, high-elevation vs λ11: deciduous SDV leaves, high-elevation | Welch two-sample t-test | -36.390462 | 185.974021 | <2.2e-16 | -0.1171522 | -0.1051033 | -0.1111277 |
| **comparison** | **statistic** | **Effect size** | **CI lower** | **CI upper** | **N. of group1** | **N. of group2** | |
| λ00: non-SDV, non high-elevation vs λ10: deciduous SDV leaves, non high-elevation | Cohen's d | -2.9033073 | -3.2995413 | -2.5033348 | 100 | 100 | |
| λ00: non-SDV, non high-elevation vs λ01: non deciduous SDV leaves, high-elevation | Cohen's d | -1.6263236 | -1.944843 | -1.3046755 | 100 | 100 | |
| λ10: deciduous SDV leaves, non high-elevation vs λ11: deciduous SDV leaves, high-elevation | Cohen's d | -4.0118547 | -4.4924452 | -3.5275886 | 100 | 100 | |
| λ01: non deciduous SDV leaves, high-elevation vs λ11: deciduous SDV leaves, high-elevation | Cohen's d | -5.1463885 | -5.717605 | -4.5672622 | 100 | 100 | |

Supplementary Table 14. **Full statistical results for pairwise comparisons of leaf size among major *Berberis* clades shown in Supplementary Fig. 1d.** Reported values include the test statistic (t), degrees of freedom (df), *p* value, mean difference, Cohen's d effect size, sample sizes, and corresponding 95% confidence intervals.

| **comparison** | **statistic** | **t value** | **df** | ***p* value** | **CI lower** | **CI upper** | **Mean difference** |
|---|---|---|---|---|---|---|---|
| Clade 1 vs Clade 1+3 | Welch two-sample t-test | 1.75230913 | 51.2947594 | 0.0857 | -25.738579 | 379.486861 | 176.874141 |
| Clade 5 vs Clade 6 | Welch two-sample t-test | 5.32498756 | 39.8509217 | 4.22e-06 | 312.394004 | 694.662298 | 503.528151 |
| Clade 6 vs Clade 1+3 | Welch two-sample t-test | 8.61047721 | 117.79112 | 3.79e-14 | 251.527424 | 401.780596 | 326.65401 |
| **comparison** | **statistic** | **Effect size** | **CI lower** | **CI upper** | **N. of group1** | **N. of group2** | |
| Clade 1 vs Clade 1+3 | Cohen's d | 0.39700336 | 0.02875366 | 0.76387734 | 40 | 104 | |
| Clade 5 vs Clade 6 | Cohen's d | 1.66250751 | 1.26410073 | 2.05691402 | 40 | 130 | |
| Clade 6 vs Clade 1+3 | Cohen's d | 1.24389594 | 0.96118966 | 1.5243336 | 104 | 130 | |

Supplementary Table 15. **Full statistical results for pairwise comparisons of leaf major vein density among major *Berberis* clades shown in Supplementary Fig. 1d.** Reported values include the test statistic (t), degrees of freedom (df), *p* value, mean difference, Cohen's d effect size, sample sizes, and corresponding 95% confidence intervals.

| **comparison** | **statistic** | **t value** | **df** | ***p* value** | **CI lower** | **CI upper** | **Mean difference** |
|---|---|---|---|---|---|---|---|
| Clade 1 vs Clade 1+3 | Welch two-sample t-test | -3.0264864 | 140.60378 | 0.00294 | -0.0353114 | -0.0074068 | -0.0213591 |
| Clade 5 vs Clade 6 | Welch two-sample t-test | -11.128244 | 51.4701171 | 2.62E-15 | -0.0601192 | -0.0417463 | -0.0509328 |
| Clade 6 vs Clade 1+3 | Welch two-sample t-test | -5.185894 | 115.320061 | 9.29E-07 | -0.0408694 | -0.0182781 | -0.0295737 |
| **comparison** | **statistic** | **Effect size** | **CI lower** | **CI upper** | **N. of group1** | **N. of group2** | |
| Clade 1 vs Clade 1+3 | Cohen's d | -0.4272289 | -0.7823764 | -0.0706459 | 44 | 104 | |
| Clade 5 vs Clade 6 | Cohen's d | -2.5891697 | -3.0275767 | -2.1459465 | 44 | 126 | |
| Clade 6 vs Clade 1+3 | Cohen's d | -0.7467582 | -1.0145373 | -0.4774435 | 104 | 126 | |

Supplementary Table 16. **Full statistical results for pairwise comparisons of mean temperature of coldest quarter (°C) among major *Berberis* clades shown in Supplementary Fig. 1d.** Reported values include the test statistic (t), degrees of freedom (df), *p* value, mean difference, Cohen's d effect size, sample sizes, and corresponding 95% confidence intervals.

| **comparison** | **statistic** | **t value** | **df** | ***p* value** | **CI lower** | **CI upper** | **Mean difference** |
|---|---|---|---|---|---|---|---|
| Clade 5 vs Clade 6 | Welch two-sample t-test | -0.1074681 | 84.8685499 | 0.915 | -1.313361 | 1.17866706 | -0.067347 |
| Clade 5 vs Clade 3 | Welch two-sample t-test | -11.465074 | 107.073778 | <2.2e-16 | -9.3715647 | -6.608528 | -7.9900463 |
| Clade 6 vs Clade 1 | Welch two-sample t-test | 17.8971926 | 71.7466203 | <2.2e-16 | 9.93870863 | 12.430426 | 11.1845673 |
| Clade 6 vs Clade 3 | Welch two-sample t-test | -14.600606 | 160.346359 | <2.2e-16 | -8.9943188 | -6.8510799 | -7.9226994 |
| **comparison** | **statistic** | **Effect size** | **CI lower** | **CI upper** | **N. of group1** | **N. of group2** | |
| Clade 5 vs Clade 6 | Cohen's d | -0.0182271 | -0.3436779 | 0.30727422 | 50 | 132 | |
| Clade 5 vs Clade 3 | Cohen's d | -2.0361021 | -2.4633134 | -1.6035311 | 50 | 82 | |
| Clade 6 vs Clade 1 | Cohen's d | 3.09852356 | 2.61894941 | 3.57312267 | 42 | 132 | |
| Clade 6 vs Clade 3 | Cohen's d | -2.0961339 | -2.4346291 | -1.754311 | 132 | 82 | |

## Supplementary references


1. Liu, J., Milne, R. I., Zhu, G.-F., Spicer, R. A., Wambulwa, M. C., Wu, Z.-Y., Boufford, D. E., Luo, Y.-H., Provan, J., Yi, T.-S., Cai, J., Wang, H., Gao, L.-M. & Li, D.-Z. Name and scale matter: Clarifying the geography of Tibetan Plateau and adjacent mountain regions. *Global Planet. Change* **215**,103864 (2022).

2. Holten, J. I. Altitude ranges and spatial patterns of alpine plants in northern Europe. In *Alpine Biodiversity in Europe* (eds Nagy, L., Grabherr, G., Körner, C. & Thompson, D. B. A.) 173–184 (Springer, 2003).

3. Aeschimann, D., Lauber, K., Moser, D. M. & Theurillat, J. P. *Flora alpina: Atlas des 4,500 plantes vasculaires des Alpes* (Belin, 2004).

4. Xu, B. & Li, Z. M. *Seed Plants in the Alpine Subnival Belt of the Hengduan Mountains* (Science Press, 2014).

5. Manish, K. & Pandit, M. K. Geophysical upheavals and evolutionary diversification of plant species in the Himalaya. *PeerJ* **6**, e5919 (2018).

6. Madriñán, S., Cortés, A. J., Richardson, J. E.. Páramo is the world's fastest evolving and coolest biodiversity hotspot. *Front. Genet.* **4**, 192 (2013).

7. Lu, X., Zheng, X., Liang, E. et al. Patterns, dynamics and drivers of alpine treelines and shrublines. *Nat Rev Earth Environ* **6**, 489–502 (2025).

8. Körner, C. *Alpine Plant Life: Functional Plant Ecology of High Mountain Ecosystems*, 3rd edn (Springer Nature, 2021).

9. Kreuzer, M., Howard, C., Adhikari, B., Pendry, C. A. & Hawkins, J. A. Phylogenomic approaches to DNA barcoding of herbal medicines: developing clade-specific diagnostic characters for *Berberis*. *Front. Plant Sci.* **10**, 586 (2019).

10. Adhikari, B., Milne, R. I., Pennington, R. T., Särkinen, T. & Pendry, C. A. Systematics and biogeography of *Berberis* s.l. inferred from nuclear ITS and chloroplast ndhF gene sequences. *Taxon* **64**, 39–48. (2015).

11. Kim, Y. D., Kim, S. H. & Landrum, L. R. Taxonomic and phytogeographic implications from ITS phylogeny in *Berberis* (Berberidaceae). *J. Plant Res.* **117**, 175–182 (2004).

12. Jin, J. J., Yu, W. B., Yang, J. B., Song, Y., dePamphilis, C. W., Yi, T. S. & Li, D. Z. GetOrganelle: a fast and versatile toolkit for accurate de novo assembly of organelle genomes. *Genome Biol.* **21**, 241 (2020).

13. Shang, H. Y., Jia, K. H., Li, N. W., Zhou, M. J., Yang, H., Tian, X. L., Ma, Y. P. & Zhang, R. G. Phytop: a tool for visualizing and recognizing signals of incomplete lineage sorting and hybridization using species trees output from ASTRAL. *Hortic Res.* **12**, uhae330 (2024).

14. Solís-Lemus, C. & Ané, C. Inferring Phylogenetic networks with maximum pseudolikelihood under incomplete lineage sorting. *PLoS Genet.* **12**, e1005896 (2016).

15. Zhang, C., Rabiee, M., Sayyari, E. & Mirarab, S. ASTRAL-III: polynomial time species tree reconstruction from partially resolved gene trees. *BMC Bioinformatics* **19**, 153.

16. Wright, I. J., Dong, N., Maire, V., et al. Global climatic drivers of leaf size. *Science* **357**, 917–921 (2017).

17. Wang, R., Chen, H., Liu, X., Wang, Z., Wen, J. & Zhang, S. Plant phylogeny and growth form as drivers of the altitudinal variation in woody leaf vein traits. *Front. Plant Sci.* **10**, 1735 (2020).

18. Yao, G.-Q., Qi, S.-H., Li, Y.-R., Duan, Y.-N., Jiang, C., Nie, Z.-F., Liu, X.-D., Hasan, M. M., Xu, D.-H., Jing, W.-M., McAdam, S. & Fang, X.-W. The combination of high leaf hydraulic safety and water use efficiency allows alpine shrubs to adapt to high-altitude habitats. *Funct. Ecol.* **38**, 2349–2362 (2024).

19. Sack, L. & Scoffoni, C. Leaf venation: structure, function, development, evolution, ecology and applications in the past, present and future. *New Phytol* **198**, 983–1000 (2013).

20. Bai, K., He, C., Wan, X. & Jiang, D. Leaf economics of evergreen and deciduous tree species along an elevational gradient in a subtropical mountain. *AoB PLANTS* **7**, plv064 (2015).

21. Edwards, E. J., Chatelet, D. S., Chen, B.-C., Ong, J.-Y., Tagane, S., Kanemitsu, H., Tagawa, K., Teramoto, K., Park, B., Chung, K.-F., Hu, J.-M., Yahara, T. & Donoghue, M. J. Convergence, consilience, and the evolution of temperate deciduous forests. *Am. Nat.* **190**, S87–S104 (2017).